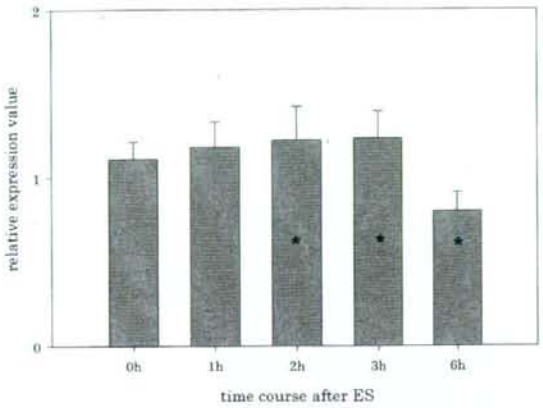

FIGURE 2. Relative gene expressions of BDNF after ES at 10 mA determined by RT-PCR. The relative values are presented as the mean multiple of change (*x*-fold) ± SD calculated from six separate experiments. Statistical analysis was performed by the Wilcoxon signed rank test (*$P < 0.05$).

Upregulation of BDNF mRNA by ES in Cultured Müller Cells

The time course of transcriptional induction of BDNF by ES was determined by RT-PCR (Fig. 2). The mRNA level was significantly increased by approximately 1.2-fold at 2 and 3 hours after ES over that of the control, and the level was decreased at 6 hours.

Upregulation of BDNF Protein by ES in Cultured Müller Cells

Because the relative value of the mRNA of BDNF increased at 2 and 3 hours after ES, the protein level of BDNF was determined from 3 hours after ES. The level in the ES group was compared to that in the control group at each time point (Fig. 3). The absolute values of the extracellular proteins of BDNF ranged from 10.2 to 129.6 pg and the intracellular values from 25.5 to 151.3 pg. The intracellular level of BDNF protein was often higher than that of extracellular protein. These relatively large variations were probably due to the different number of cultured Müller cells between the experimental runs.

The intracellular protein level of BDNF in the experimental cells was significantly increased (>1.4-fold) at 6 hours after ES compared with that in the control cells, whereas the extracellular level did not change significantly at any time point. The total protein was significantly upregulated (by ~1.3-fold) at 6 hours after ES.

Suppression of BDNF mRNA by Blocking L-VDCCs in Cultured Müller Cells

In earlier work, we showed that ES induced the transcription of IGF-1 by Ca^{2+} influx via L-VDCCs in cultured Müller cells.[13] Because Ca^{2+} ions are one of the common second messengers,[14] we hypothesized that the transcriptional induction of BDNF also depends largely on the Ca^{2+} influx through L-VDCCs. A common pharmacologic hallmark of L-VDCCs is their sensitivity to dihydropyridines.[24] Thus, the gene expression of BDNF was determined at 3 hours after ES by RT-PCR in Müller cells loaded with 1 μM nifedipine, a dihydropyridine calcium channel blocker (Fig. 4).

The mRNA level of BDNF was approximately 0.5-fold at 0 mA with nifedipine and 0.4-fold at 10 mA with nifedipine compared with that of 0 mA (control). Statistical significance

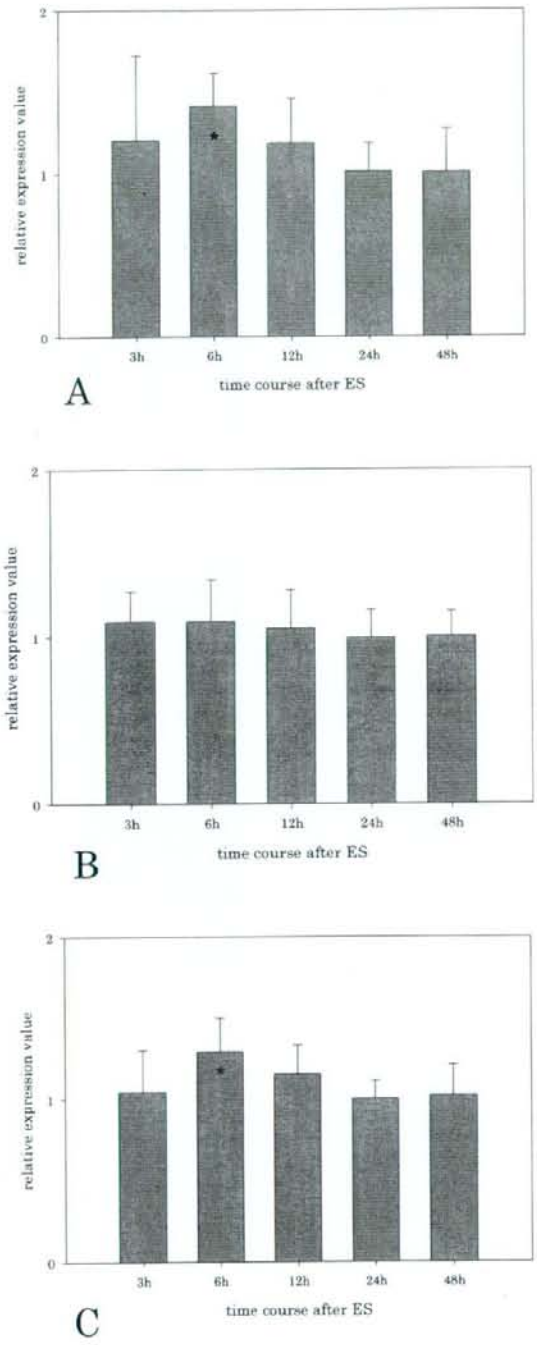

FIGURE 3. Relative protein expressions of BDNF after ES at 10 mA determined by ELISA. The relative values are presented as the mean multiple of change (*x*-fold) ± SD calculated from six separate experiments. Statistical analysis was performed by Wilcoxon signed rank test (*$P < 0.05$). (**A**) Intracellular protein level of BDNF. The absolute levels of intracellular BDNF ranged from 25.5 to 151.3 pg. (**B**) Extracellular level of BDNF. The absolute extracellular level of BDNF ranged from 10.2 to 129.6 pg. (**C**) Total level of BDNF. The absolute level of total BDNF ranged from 60.0 to 249.3 pg.

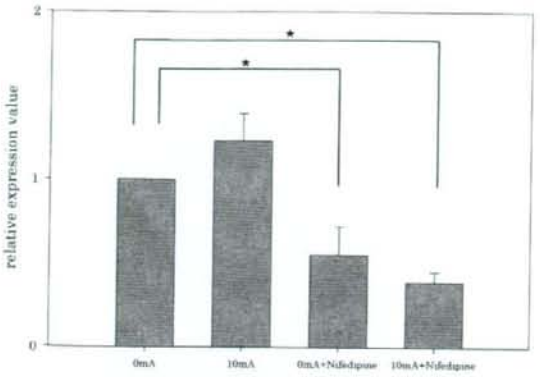

FIGURE 4. Relative gene expressions of BDNF with or without 1 μM nifedipine at 3 hours after 10 mA ES, determined by RT-PCR. The relative data are presented as the mean multiples of change (x-fold) ± SD in 12 separate experiments. Statistical analysis was performed by Kruskal-Wallis one-way ANOVA on ranks, followed by the Dunn test (*$P < 0.05$).

was detected among these four groups ($P = < 0.001$; Kruskal-Wallis one-way ANOVA on ranks), and the levels after exposure to nifedipine were significantly lower than that with 0 mA ($P < 0.05$; Dunn's method). These results indicated that the transcription of BDNF in cultured Müller cells was upregulated by ES, was most likely due to Ca^{2+} influx into the cells via L-VDCCs, and was downregulated by the application of nifedipine, which prevented Ca^{2+} influx via L-VDCCs.

DISCUSSION

To investigate the direct effect of ES on the production of neurotrophic factors from Müller cells, ES was applied to cultured Müller cells. The major findings were that both the message and protein levels of BDNF in cultured Müller cells were upregulated by ES, and that the transcriptional induction of BDNF is fully depressed by the application of an L-VDCC blocker. These findings suggest that the transcriptional induction by ES depends largely on Ca^{2+} influx through L-VDCCs.

Although BDNF was first purified from brain cells,[25] it has been shown to play crucial roles, not only in CNS[26–28] but also in the retina. Recent studies have demonstrated that BDNF promoted the survival of RGCs in different models.[29–33] Furthermore, Paskowitz et al.[34] demonstrated that BDNF increased photoreceptor survival after verteporfin photodynamic therapy, indicating that BDNF had a neuroprotective effect on the photoreceptors. These findings support the conclusion that BDNF acts as a neurotrophic agent in the retina.

However, one crucial question regarding the clinical application of BDNF is how to deliver it to the retinal neurons. Previous studies[29–34] have demonstrated that exogenous BDNF, delivered by intravitreous injections, had a protective effect on retinal neurons. However, exogenous BDNF had a transient and limited protective effect, and repeated applications were necessary, which can have adverse effects on the retina. On this point, we have already developed a system of transcorneal ES to the retina and showed the protective effect on the eyes with optic nerve diseases without serious complications.[35] These results indicate the possibility that ES may safely induce the production of endogenous BDNF from Müller cells to promote the survival of retinal neurons.

In this study, the extracellular protein level of BDNF did not increase at any time point. The reason for this is still not clear, but one possibility is that BDNF behaves as an autocrine factor in cultures of pure Müller cells. An earlier study demonstrated that Müller cells not only synthesize BDNF but also express TrkB, the specific receptor of BDNF.[36] These results indicate that BDNF secreted from Müller cells may be expanded by an autocrine mechanism and that the transcriptional induction of BDNF may be suppressed at 6 hours by negative feedback of the increased protein of BDNF.

The mechanism of how ES stimulates L-VDCCs in cultured Müller cells is not fully understood. It is well known that Ca^{2+}-regulated gene expression plays a critical role in diverse neural functions and that the activation of L-VDCCs is required for depolarization-mediated gene induction.[20] Most studies that have examined mechanisms of activity-dependent gene expression have used chronic membrane depolarization to raise intracellular calcium levels and stimulate gene expression.[21] Further studies are needed to determine the mechanisms involved in the gene expression of BDNF by ES in Müller cells.

One of the limitations of this study is that the microarray analyses were performed at only one time point, immediately after ES. In fact, the mRNA level of BDNF determined by RT-PCR was higher at 2 and 3 hours than at 0 hours after ES, although the transcriptional induction depended mainly on Ca^{2+} influx through L-VDCCs, similar to that for IGF-1. Thus, we cannot exclude the possibility that other neurotrophic factors may have been induced by the ES.

In summary, we have demonstrated the direct effect of ES on BDNF production in cultured rat Müller cells. Our findings raise the possibility that ES may deliver endogenous BDNF from Müller cells without serious complications and promote the survival of retinal neurons.

Acknowledgments

The authors thank Takayuki Harada for crucial comments on this study.

References

1. Otori Y, Shimada S, Tanaka K, Ishimoto I, Tano Y, Tohyama M. Marked increase in glutamate-aspartate transporter (GLAST/GluT-1) mRNA following transient retinal ischemia. *Brain Res Mol Brain Res*. 1994;27:310–314.
2. Derouiche A, Rauen T. Coincidence of L-glutamate/L-aspartate transporter (GLAST) and glutamine synthetase (GS) immunoreactions in retinal glia: evidence for coupling of GLAST and GS in transmitter clearance. *J Neurosci Res*. 1995;42:131–143.
3. Kitano S, Morgan J, Caprioli J. Hypoxic and excitotoxic damage to cultured rat retinal ganglion cells. *Exp Eye Res*. 1996;63:105–112.
4. Lehre KP, Davanger S, Danbolt NC. Localization of the glutamate transporter protein GLAST in rat retina. *Brain Res*. 1997;744:129–137.
5. Matsui K, Hosoi N, Tachibana M. Active role of glutamate uptake in the synaptic transmission from retinal nonspiking neurons. *J Neurosci*. 1999;19:6755–6766.
6. Riepe RE, Norenburg MD. Muller cell localization of glutamine synthetase in rat retina. *Nature*. 1977;268:654–655.
7. Curtis DR, Watkins JC. The excitation and depression of spinal neurones by structurally related amino acids. *J Neurochem*. 1960;6:117–141.
8. Seki M, Tanaka T, Sakai Y, et al. Müller cells as a source of brain-derived neurotrophic factor in the retina: noradrenaline upregulates brain-derived neurotrophic factor levels in cultured rat Müller cells. *Neurochem Res*. 2005;30:1163–1170.
9. Wilson RB, Kunchithapautham K, Rohrer B. Paradoxical role of BDNF: $BDNF^{+/-}$ retinas are protected against light damage-mediated stress. *Invest Ophthalmol Vis Sci*. 2007;48:2877–2886.
10. Cao W, Wen R, Li F, Cheng T, Steinberg RH. Induction of basic fibroblast growth factor mRNA by basic fibroblast growth factor in Müller cells. *Invest Ophthalmol Vis Sci*. 1997;38:1358–1366.
11. Harada T, Harada C, Nakayama N, et al. Modification of glial-neuronal cell interactions prevents photoreceptor apoptosis during light-induced retinal degeneration. *Neuron*. 2000;26:533–541.

12. Morimoto T, Miyoshi T, Matsuda S, Tano Y, Fujikado T, Fukuda Y. Transcorneal electrical stimulation rescues axotomized retinal ganglion cells by activating endogenous retinal IGF-1 systems. *Invest Ophthalmol Vis Sci*. 2005;46:2147–2155.
13. Sato T, Fujikado T, Morimoto T, Matsushita K, Harada T, Tano Y. Effect of electrical stimulation on IGF-1 transcription by L-type calcium channels in cultured retinal Müller cells. *Jpn J Ophthalmol*. 2008;52:217–223.
14. Miller RJ. Rocking and rolling with Ca2+ channels. *Trends Neurosci*. 2001;24:445–449.
15. Ou LC, Gean PW. Transcriptional regulation of brain-derived neurotrophic factor in the amygdala during consolidation of fear memory. *Mol Pharmacol*. 2007;72:350–358.
16. Sasaki M, Gonzalez-Zulueta M, Huang H, et al. Dynamic regulation of neuronal NO synthase transcription by calcium influx through a CREB family transcription factor-dependent mechanism. *Proc Natl Acad Sci USA*. 2000;97:8617–8622.
17. Ploski JE, Newton SS, Duman RS. Electroconvulsive seizure-induced gene expression profile of the hippocampus dentate gyrus granule cell layer. *J Neurochem*. 2006;99:1122–1132.
18. Follesa P, Biggio F, Gorini G, et al. Vagus nerve stimulation increases norepinephrine concentration and the gene expression of BDNF and bFGF in the rat brain. *Brain Res*. 2007;1179:28–34.
19. Geremia NM, Gordon T, Brushart TM, Al-Majed AA, Verge VMK. Electrical stimulation promotes sensory neuron regeneration and growth-associated gene expression. *Exp Neurol*. 2007;205:347–359.
20. Brosenitsch TA, Katz DM. Physiological patterns of electrical stimulation can induce neuronal gene expression by activating N-type calcium channels. *J Neurosci*. 2001;21:2571–2579.
21. Zhao R, Liu L, Rittenhouse AR. Ca2+ influx through both L- and N-type Ca2+ channels increases c-fos expression by electrical stimulation of sympathetic neurons. *Eur J Neurosci*. 2007;25:1127–1135.
22. Roque RS, Caldwell RB, Behzadian MA. Cultured Müller cells have high levels of epidermal growth factor receptors. *Invest Ophthalmol Vis Sci*. 1992;33:2587–2595.
23. Johnson MR, Wang K, Smith JB, Heslin MJ, Diasio RB. Quantitation of dihydropyrimidine dehydrogenase expression by real-time reverse transcription polymerase chain reaction. *Anal Btochem*. 2000;278:175–184.
24. Bourinet E, Mangoni ME, Nargeot J. Dissecting the functional role of different isoforms of the L-type Ca2+ channel. *J Clin Invest*. 2004;113:1382–1384.
25. Barde YA, Edgar D, Thoenen H. Purification of a new neurotrophic factor from mammalian brain. *EMBO J*. 1982;1:549–553.
26. Canals JM, Checa N, Marco S, et al. Expression of brain-derived neurotrophic factor in cortical neurons is regulated by striatal target area. *J Neurosci*. 2001;21:117–124.
27. Bifrare YD, Kummer J, Joss P, Tauber MG, Leib SL. Brain-derived neurotrophic factor protects against multiple forms of brain injury in bacterial meningitis. *J Infect Dis*. 2005;191:40–45.
28. Almeida RD, Manadas BJ, Melo CV, et al. Neuroprotection by BDNF against glutamate-induced apoptotic cell death is mediated by ERK and PI3-kinase pathways. *Cell Death Differ*. 2005;12:1329–1343.
29. Klocker N, Cellerino A, Bahr M. Free radical scavenging and inhibition of nitric oxide synthase potentiates the neurotrophic effects of brain-derived neurotrophic factor on axotomized retinal ganglion cells in vivo. *J Neurosci*. 1998;18:1038–1046.
30. Klocker N, Kermer P, Weishaupt JH, Labes M, Ankerhold R, Bahr M. Brain-derived neurotrophic factor-mediated neuroprotection of adult rat retinal ganglion cells in vivo does not exclusively depend on phosphatidyl-inositol-3'-kinase/protein kinase B signaling. *J Neurosci*. 2000;20:6962–6967.
31. Ko ML, Hu DN, Ritch R, Sharma SC, Chen CF. Patterns of retinal ganglion cell survival after brain-derived neurotrophic factor administration in hypertensive eyes of rats. *Neurosci Lett*. 2001;305:139–142.
32. Chen H, Weber AJ. BDNF enhances retinal ganglion cell survival in cats with optic nerve damage. *Invest Ophthalmol Vis Sci*. 2001;42:966–974.
33. Nakazawa T, Tamai M, Mori N. Brain-derived neurotrophic factor prevents axotomized retinal ganglion cell death through MAPK and PI3K signaling pathways. *Invest Ophthalmol Vis Sci*. 2002;43:3319–3326.
34. Paskowitz DM, Donohue-Rolfe KM, Yang H, et al. Neurotrophic factors minimize the retinal toxicity of verteporfin photodynamic therapy. *Invest Ophthalmol Vis Sci*. 2007;48:430–437.
35. Fujikado T, Morimoto T, Matsushita K, Shimojo H, Okawa Y, Tano Y. Effect of transcorneal electrical stimulation in patients with nonarteritic ischemic optic neuropathy or traumatic optic neuropathy. *Jpn J Ophthalmol*. 2006;50:266–273.
36. Oku H, Ikeda T, Honma Y, et al. Gene expression of neurotrophins and their high-affinity Trk receptors in cultured human Müller cells. *Ophthalmic Res*. 2002;34:38–42.

Adaptive Optics Fundus Camera to Examine Localized Changes in the Photoreceptor Layer of the Fovea

Yoshiyuki Kitaguchi, MD,[1] Takashi Fujikado, MD,[1] Kenichiro Bessho, MD,[1] Hirokazu Sakaguchi, MD,[2] Fumi Gomi, MD,[2] Tatsuo Yamaguchi, MS,[3] Naoki Nakazawa, BE,[3] Toshifumi Mihashi, PhD,[3] Yasuo Tano, MD[2]

Purpose: To examine highly localized photoreceptor disruptions in the fovea by a high-resolution adaptive optics (AO) fundus camera combined with Fourier-domain optical coherence tomography (FD OCT).

Design: Observational case series.

Participants: Three eyes of 3 patients who showed dark foveal spots by slit-lamp biomicroscopy.

Methods: Three patients who reported metamorphopsia but showed no changes in the retina in conventional fundus photographs were examined. High-resolution retinal images were obtained with the AO fundus camera and by FD OCT. The images were compared with the findings obtained by standard clinical tests, including Amsler charts and fluorescein angiography (FA).

Main Outcome Measures: Quantitative measurements of the area of photoreceptor disruption.

Results: Slit-lamp biomicroscopy revealed an irregularly shaped dark spot in the fovea centralis but no changes in FA in the 3 cases. The photoreceptor mosaic was absent in a highly localized area of the fovea in the images obtained by the AO fundus camera, and the photoreceptor outer segment was absent or disturbed at the corresponding area by FD OCT in all 3 cases. The horizontal and vertical sizes of the area of disturbance of the photoreceptor mosaic in the AO images in the 3 eyes were 400×200 μm, 300×120 μm, and 300×200 μm. These sizes were comparable to the photoreceptor outer segment disturbances in the OCT images which were 330×150 μm, 280×100 μm, 200×150 μm, respectively.

Conclusions: Localized OS disturbances were able to be detected in eyes with a dark foveal spot by AO fundus camera 2-dimensionally and by FD OCT axially. The good correspondence of the sizes of the area of photoreceptor disturbances obtained by AO images to those by FD OCT images indicate that the AO images can be used to evaluate and follow the 2-dimensional area of focal changes of the photoreceptors in the fovea quantitatively.

Financial Disclosure(s): Proprietary or commercial disclosure may be found after the references.
Ophthalmology 2008;115:1771–1777 © 2008 by the American Academy of Ophthalmology.

With current advanced retinal imaging instruments, small focal changes of the retina can be detected and measured more accurately. These findings can help in determining the cause of unexplained visual symptoms and visual loss. For example, the retina of patients at the early phase of macular dystrophy appears ophthalmoscopically normal.[1–6] However, examination of optical coherence tomography (OCT) images showed that the retina was thinner at the macular area and that the decrease in thickness was correlated with the reduced visual acuity.[4] With additional improvements in the axial resolution by ultra–high-resolution OCT, several studies have shown a good correlation between the disruption of the photoreceptor inner segment/outer segment (IS/OS) junction and the decrease in visual acuity.[7–10] Ultra–high-resolution OCT, or Fourier-domain (FD) OCT, has an axial resolution of approximately 3 to 5 μm,[9–12] which is significantly better than the axial resolution of approximately 10 μm with the standard OCT. This increased resolution results in better delineation of the retinal architecture and helps in identifying pathologic changes in the microstructure of the retina, especially the photoreceptor layer.[9–11]

A disturbance of IS/OS junction has been reported in cases of postoperative retinal detachment, central serous chorioretinopathy, and retinal dystrophy.[7,8,10,11,13,14] Some studies have found a good correlation between the disturbance of IS/OS junction and the visual acuity.[4,7,10,11]

One problem with conventional OCT is its low transverse resolution. Generally, the transverse resolution of OCT is on the order of 20 μm, which exceeds the cone mosaic spacing of 5 to 10 μm. Two reasons for this limitation are the ocular aberrations and saccadic eye movements. The A-scan technologies adopted in OCT are not suited for obtaining transverse information in both the x- and y-directions in a short acquisition time, and obtaining motion-artifact–free 2-dimesional transverse images of the cone mosaic is not possible.[16]

Adaptive optic (AO) systems seem to be well suited to overcome these problems. An AO system consists of a wavefront sensor to measure ocular aberrations and a de-

ISSN 0161-6420/08/$–see front matter
doi:10.1016/j.ophtha.2008.03.026

formable mirror to compensate for these aberrations. Correcting the ocular aberrations with the AO system can improve the transverse resolution to less than 2 μm, which is necessary to image individual photoreceptors in the living retina.[16–20] Because transverse 2-dimensional images of the retina can be obtained with the AO system, precise detection and measurements of small lesions can be made. Thus, the AO images of patients with cone dystrophy have been reported to have a patchy configuration because of photoreceptor dropout.[21–23] The limitation of the AO system is its low axial resolution. The axial resolution of AO system is approximately 100 μm, even when it is coupled with a scanning laser ophthalmoscope.[19] It is even greater with conventional flood-illumination fundus photography.

Because of the complementary aspects of FD OCT and AO, that is, high axial resolution with FD OCT and high transverse resolution with the AO system, it theoretically would be valuable to combine both instruments to evaluate small focal photoreceptor disruptions. However, the authors have not found a publication that used both systems to compare the images obtained with FD OCT and those obtained with the AO system. The authors have developed a compact, clinically friendly AO fundus camera using a liquid crystal phase modulator. With this instrument, they have been able to show the increased cone spacing in myopic eyes.[24] The purpose of this study was to determine the cause of dark spots in the fovea of 3 patients with metamorphopsia. In all 3 patients, the fundus appeared ophthalmoscopically normal and the photographs obtained by conventional fundus photography also demonstrated normal results. These retinas were examined with their custom-built AO fundus camera, and the images were compared with the OCT images.

Patients and Methods

Patients

Three consecutive patients who reported metamorphopsia but whose photographs of the ocular fundus by standard fundus photography demonstrated normal results were studied. All patients had visited Osaka University Hospital between January and June 2006. The research protocol was approved by the Institutional Review Board of the Osaka University Medical School, and the procedures conformed to the tenets of the Declaration of Helsinki. After the nature and possible consequences of the study were explained, written informed consent was obtained from all patients.

Procedures

All patients underwent a comprehensive ophthalmologic examination, including the measurement of best-corrected visual acuity (BCVA), Amsler chart, fundus photography, and slit-lamp biomicroscopy of the fundus. They also underwent examinations by FD OCT (RTVue-100; Optovue, Inc., Fremont, CA) and a custom-built AO fundus camera.[24] All 3 patients also underwent fluorescein angiography (FA) and indocyanine green angiography (ICGA).

Adaptive Optic Fundus Camera

A detailed description of the custom-built AO fundus camera has been published.[24] The principle of this flood illumination AO fundus camera was similar to that reported by Roorda and Williams.[17] Briefly, the main components of the camera were a nematic liquid crystal phase modulator (X8267–12; Hamamatsu Photonics, Hamamatsu, Japan), a Hartmann-Shack wavefront sensor (28×28 lenslets; specially made by Topcon, Co., Tokyo, Japan), and a scientific charge-coupled device digital camera (C9100–02; Hamamatsu Photonics).

The wavefront sensor measured the ocular wavefront up to the eighth Zernike order, and the phase modulator compensated for the measured wavefront aberrations. The system also is equipped with coaxial, 8-degree–wide viewing optics to identify the location and orientation of the highly magnified retinal images being observed.

Topical tropicamide (0.5%) and phenylephrine (0.5%) were used to dilate the pupil and to paralyze the ciliary muscle. The retina was illuminated with a 2-ms flash (635-nm wavelength) from a xenon arc lamp, and a retinal image was obtained with a 6-mm–diameter exit pupil. The patient was instructed to fixate a designated location on a target. Frame averaging was performed using custom software (Topcon) to improve the quality of the image. Overlapping images were merged using Photoshop (Adobe Systems, Inc., San Jose, CA). To identify the fovea, a montage of the AO images was made and superimposed on the fundus photographs and the fundus projection of OCT images.

Case Reports

Patient 1. A 39-year-old man reported metamorphopsia in his left eye which began 3 months earlier. His BCVA was 20/15 in both eyes. Ophthalmoscopy showed that the ocular fundus appeared normal in both eyes (Fig 1A). Slit-lamp biomicroscopy showed an irregularly shaped dark spot in the fovea centralis of the left eye. Amsler chart examination showed a localized area of metamorphopsia just below the fixation point.

Fourier-domain OCT demonstrated a disturbance of the IS/OS junction and OS layer (between second and third line of FD OCT) of approximately 330 μm on the horizontal scan and 150 μm on the vertical scan. The external limiting membrane layer was intact (Fig 1B,C).

The AO image showed a dark area, that is, an absence of the cone mosaic, at the fovea just above the fixation point. The shape of dark area was geographic, and the size was approximately 350 μm horizontally and 160 μm vertically (Fig 1D–F).

Patient 2. A 39-year-old man reported blurred vision and metamorphopsia in his right eye of 2 years' duration. His BCVA was 20/60 in the right eye and 20/20 in the left eye. He had been diagnosed with keratoconus in his right eye, but his vision did not improve after wearing a hard contact lens.

The ocular fundus appeared normal in fundus photographs (Fig 2A). Slit-lamp biomicroscopy showed an abnormal reflex in the macula and an irregularly shaped dark spot in the fovea centralis of the right eye. Amsler chart examination showed a central scotoma. Fluorescein angiography and ICGA did not show any abnormal findings (Fig 2B).

Fourier-domain OCT demonstrated a defect in the OS layer in the fovea that was located just under the IS/OS layer. The size of the defect was 280 μm on the horizontal scan and 100 μm on the vertical scan. The IS/OS junction was preserved but the intensity was slightly lower. The external limiting membrane and the RPE layers appeared to be normal (Fig 2C,D).

The AO image indicated a disappearance of the cone mosaic at the fovea. The dark area was oval, and the size was 300 μm horizontally and 120 μm vertically (Fig 2E–G).

Patient 3. A 62-year-old man reported metamorphopsia in his left eye of 6 months' duration. His BCVA was 20/200 in the right eye and 20/22 in the left eye. No abnormality was found in the ocular fundus in the conventional fundus photographs (Fig 3A). Slit-lamp biomicroscopy showed an irregularly shaped dark spot in the fovea centralis of the left eye. Amsler chart examination indicated a localized area of metamorphopsia just below the fixation point. The FA and ICGA results were normal (Fig 3B).

Fourier-domain OCT demonstrated an elevation of the external limiting membrane. The photoreceptor OS and IS/OS junction were not detected over an area of 200 μm on the horizontal scan and 150 μm on the vertical scan (Fig 3C,D).

The AO image demonstrated the disappearance of the cone mosaic at the foveal zone. At the fovea centralis, a relatively high reflective area without cone mosaic was observed. The area of the absence of foveal cones was approximately 300 μm horizontally and 200 μm vertically (Fig 3E,F).

Results

All 3 patients had metamorphopsia unilaterally, and the BCVA ranged 20/200 to 20/15 in the affected eye. The Amsler chart examination showed localized metamorphopsia in 2 eyes and a central scotoma in 1 eye. The ocular fundus appeared to be normal in standard fundus photographs, but slit-lamp biomicroscopy revealed an irregularly shaped dark spot in the fovea centralis in the 3 cases. Fluorescein angiography and ICGA did not show any abnormal findings in any cases.

Fourier-domain OCT demonstrated an absence of the OS and IS/OS junction of the photoreceptors in 1 case and an absence or disturbance of the OS but preservation of the IS/OS junction in 2 cases. The AO images indicated the absence of the cone mosaic in the foveal zone in all 3 cases. The horizontal and vertical sizes of the area of the absence of the photoreceptor mosaic in the AO images in the 3 eyes (400×200 μm, 300×120 μm, and 300×200 μm) were comparable with the sizes of the photoreceptor OS disturbances in the OCT images (330×150 μm, 280×100 μm, 200×150 μm, respectively).

Discussion

This study examined the FD OCT and AO images in patients who showed localized disturbances in the photoreceptor layer. To the best of the authors' knowledge, this is the first study that compares the FD OCT and AO images in the same patient. A localized disappearance of the photoreceptor mosaic was observed in the photographs of the fovea obtained by the AO fundus camera in all 3 cases. The horizontal and vertical sizes of the area of the loss of the photoreceptor mosaic in the AO images were comparable with the area of the OS disturbance in the OCT images. In patient 3, the IS/OS junction and OS were also not detected, but in patients 1 and 2, the IS/OS line was preserved, although the intensity was slightly lower than normal. These results suggested that the dark area seen by slit-lamp biomicroscopy corresponded with an absence of the photoreceptor mosaic in the AO images and with the disturbed photoreceptor OS in the OCT images.

The origin of the high reflectance cone mosaic in the AO fundus camera is reported to be from both the IS/OS junction and the OS in the normal retina.[15] However, based on the results from patient 1, a possibility exists that the OS is more involved in the reflectance of photoreceptor mosaic than the IS/OS junction in the AO images. This hypothesis corresponds with the results of a recent report using AO OCT, in which the cone mosaic is observed clearly at the level of Verhoeff's membrane (the third blight line of FD OCT), where the tip of the cone photoreceptor OS is enveloped by microvilli.[25]

In patients with a macular hole, metamorphopsia is a frequently reported symptom. In the early stage of macular hole, morphologic changes are observed not only in the photoreceptor layer, but also in the inner retinal layers because of the tangential traction on the retinal surface. All of the patients reported metamorphopsia, but the lesion was confined to only the photoreceptor layer and was in a very restricted area in the fovea.

Recently, a new clinical entity termed *foveal spot* or *macular microhole* has been proposed.[26,27] In this lesion, the patient has a mildly reduced visual acuity, a central scotoma, and metamorphopsia, and ophthalmoscopy shows a foveal defect with a red appearance and well-defined margins. The size of the lesion is approximately 100 μm and seems to be intraretinal. Conventional OCT3 images (Stratus model 3000; Carl Zeiss Meditec, Humphrey Division, Dublin, CA) show an abnormality of the outer retina, a defect of retinal pigment epithelium, or both.[27] All 3 of the eyes had an apparently normal ocular fundus by conventional fundus photography, but slit-lamp biomicroscopy showed an irregularly shaped dark spot in the fovea centralis. Thus, the 3 eyes may be included in the category of macular microhole or foveal spot. The decrease in the visual acuity or an increase in the area of metamorphopsia should be reflected in the size of the dark area in AO fundus image, and thus may be helpful to evaluate the progression of a disease quantitatively.

The limitation of this study is that the fovea could not be resolved accurately with the AO system. The AO system allows a transverse resolution of 2 μm, but the photoreceptors in the fovea are smaller than the resolution limit.[16–20] Because of this, it is difficult to identify the individual cones in the fovea centralis in the AO images. However, because the dark area is not observed in the central fovea in normal eyes, the dark area at or around the central fovea can be assumed to be the area of photoreceptor loss or disruption.

In conclusion, the AO fundus camera can acquire 2-dimensional images of the retina with a resolution of approximately 2 μm. This resolution allows the detection of highly localized disturbances of the photoreceptor cells that can correlate with the high-resolution images obtained by FD OCT. Combining the AO fundus camera and FD OCT images can be valuable to assess photoreceptor disruptions, especially in eyes with a small focal foveal lesion. The findings in these 3 patients indicate that patients reporting metamorphopsia may have a localized disruption the of photoreceptor cells in the fovea.

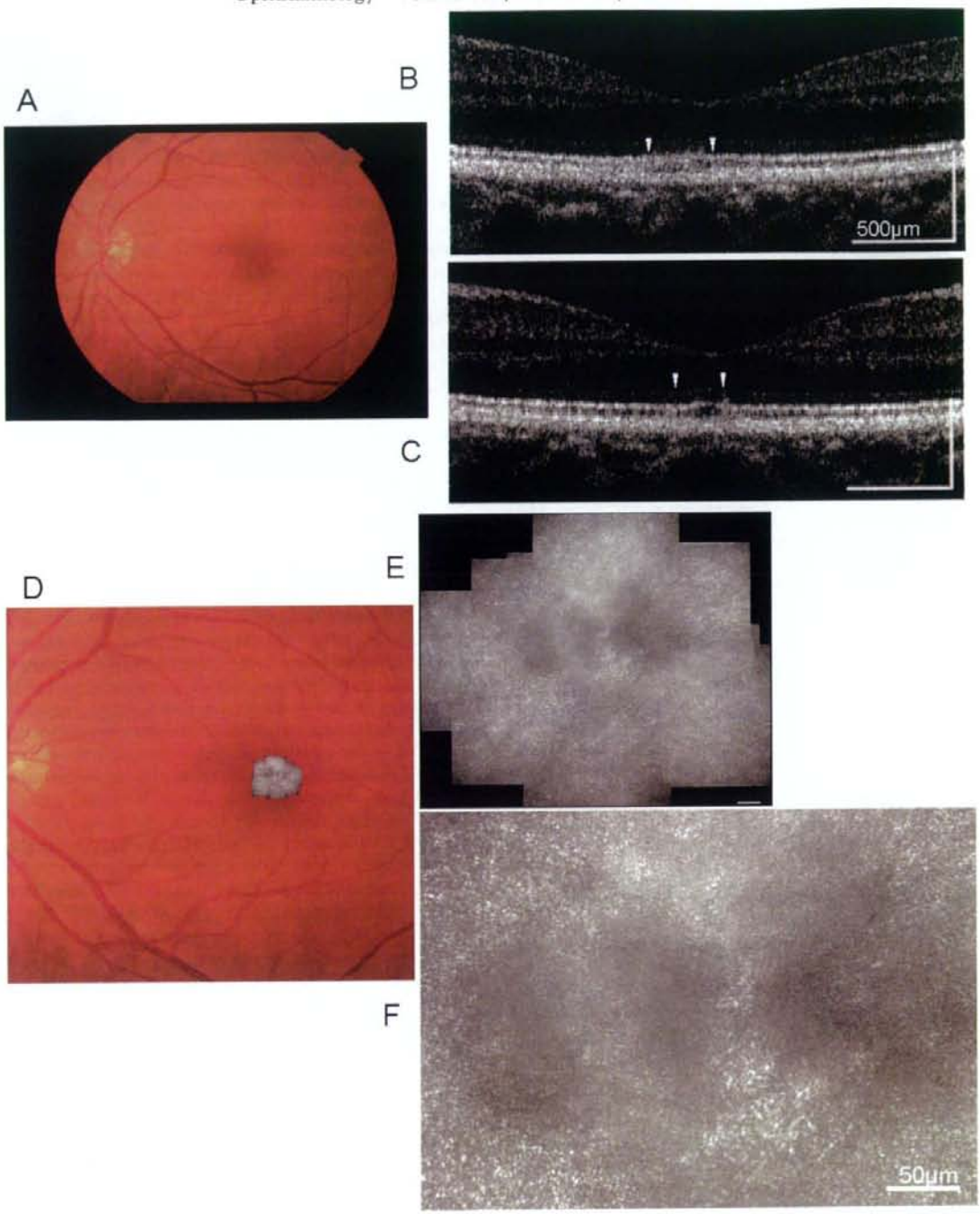

Figure 1. Images from the left eye of patient 1, who sought treatment for metamorphopsia. **A**, Fundus photograph showing normal appearance. **B**, Fourier-domain optical coherence tomography image (5-mm horizontal scan) demonstrating the disturbance of the inner segment/outer segment (IS/OS) junction and outer segment (OS) layer (between the second and third lines) for approximately 330 μm. **C**, Fourier-domain optical coherence tomography vertical scan showing the disturbance of the IS/OS junction and OS layer for approximately 150 μm. The arrowhead in **B** and **C** point to the area of IS/OS and OS disturbances. The horizontal bars in **B** and **C** represent 500 μm. **D**, Montage of adaptive optics (AO) image superimposed on the fundus photograph. **E**, Montage of adaptive optics image (low magnification). **F**, Magnified AO image of the fovea showing a dark area (disappearance of cone mosaic) at the fovea just above the fixation point. The shape of dark area was geographic and the size was approximately 350 μm horizontally and 180 μm vertically. The horizontal bars in **E** and **F** represent 50 μm.

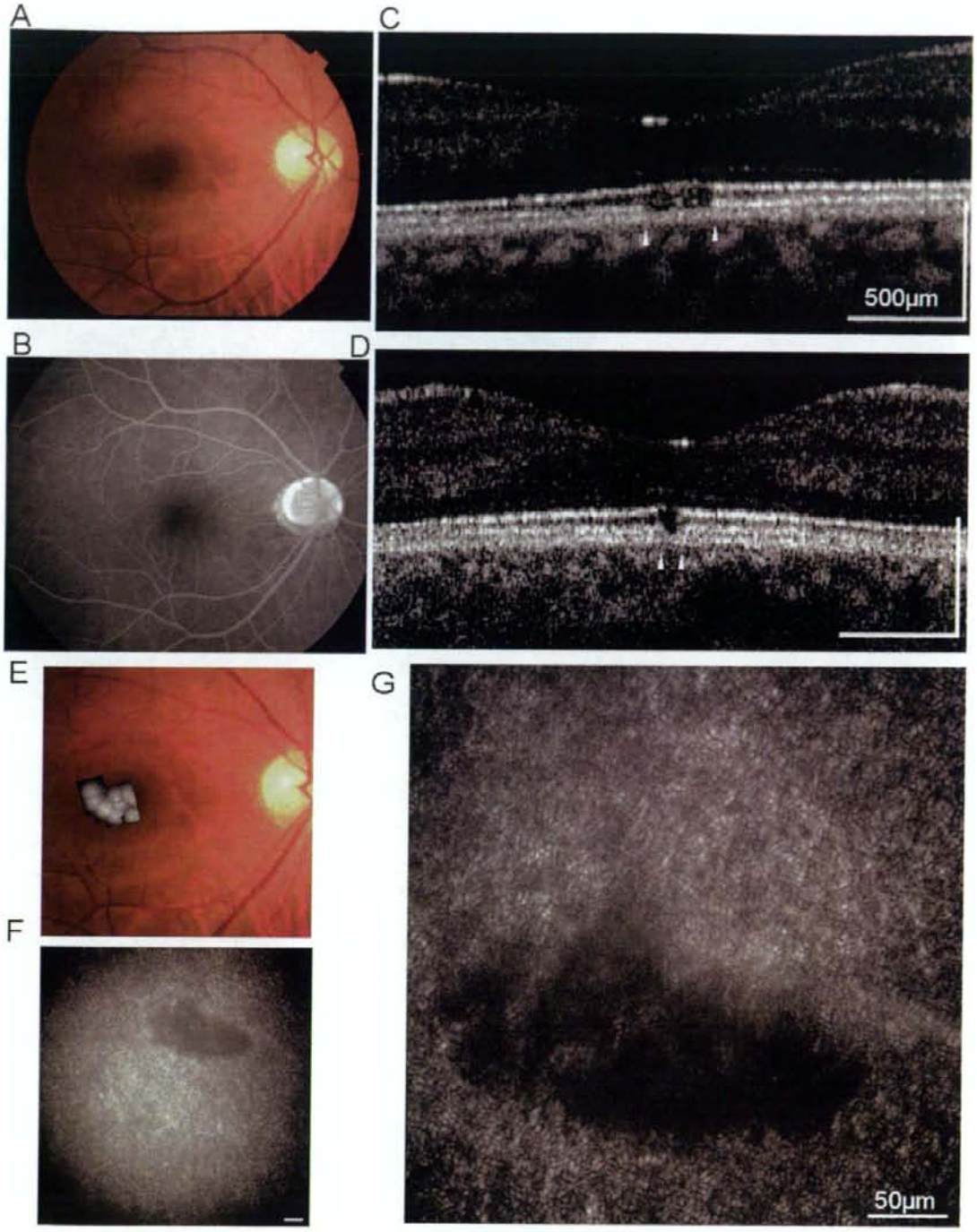

Figure 2. Images from the right eye of patient 2, who sought treatment for metamorphopsia. **A**, Fundus photograph showing that the retina appears to be normal. **B**, Early-phase fluorescein angiography image showing normal results. **C** and **D**, Fourier-domain optical coherence tomography images demonstrating a defect of outer segment (OS) layer in the fovea that was located just beneath the inner segment/OS junction. The size of the defect was (**C**) 280 μm on the horizontal scan and (**D**) 100 μm on the vertical scan. The IS/OS line was preserved but the intensity was slightly low. The arrowhead in **C** and **D** points to the area of OS defect. The horizontal bars in **C** and **D** represent 500 μm, and the vertical bars represent 200 μm. **E**, Montage of adaptive optics (AO) image superimposed on the fundus photograph. **F**, adaptive optics image (low magnification). **G**, Magnified AO image of the fovea showing a dark oval-shaped area (disappearance of cone mosaic) with a size of 300 μm horizontally and 120 μm vertically. The horizontal bars in **F** and **G** represent 50 μm.

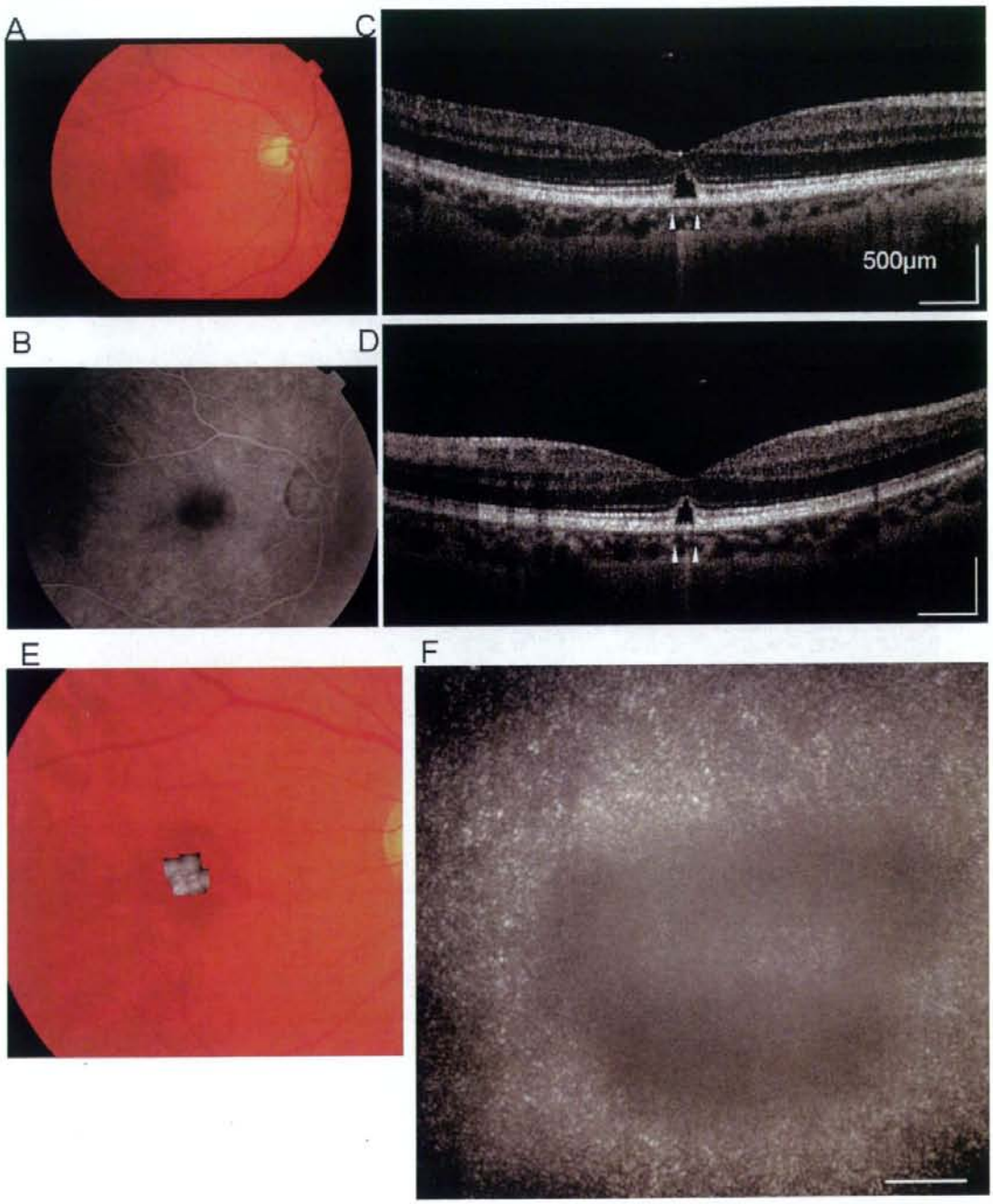

Figure 3. Images from the right eye of patient 3, who sought treatment for metamorphopsia. **A**, Fundus photograph showing normal appearance. **B**, Early-phase of fluorescein angiography image showing normal results. **C** and **D**, Fourier-domain optical coherence tomography images demonstrating the elevation of the external limiting membrane. Photoreceptor outer segment (OS) and inner segment/OS junction are not present in an area of (**C**) 200 μm on the horizontal scan and (**D**) 150 μm on the vertical scan. The arrowhead in **C** and **D** indicates the area of OS defect. The horizontal bars in **C** and **D** represent 500 μm, and the vertical bars represent 200 μm. **E**, Montage of adaptive optics (AO) image superimposed on the fundus photograph. **F**, Magnified image of AO image in the fovea demonstrating a dark oval-shaped area (disappearance of cone mosaic) with a size of 300 μm horizontally and 200 μm vertically. At the fovea centralis, a slightly high reflective area without cone mosaic was observed. The horizontal bars in **F** represent 50 μm.

References

1. Brockhurst RJ, Sandberg MA. Optical coherence tomography findings in occult macular dystrophy. Am J Ophthalmol 2007; 143:516–8.
2. Kondo M, Ito Y, Ueno S, et al. Foveal thickness in occult macular dystrophy. Am J Ophthalmol 2003;135:725–8.
3. Benhamou N, Souied EH, Zolf R, et al. Adult-onset foveomacular vitelliform dystrophy: a study by optical coherence tomography. Am J Ophthalmol 2003;135:362–7.
4. Sandberg MA, Brockhurst RJ, Gaudio AR, Berson EL. The association between visual acuity and central retinal thickness in retinitis pigmentosa. Invest Ophthalmol Vis Sci 2005;46: 3349–54.
5. Samsel A, Drobecka-Brydak E, Godowska-Brydak E, et al. Optical coherence tomography in Stargardt's dystrophy [in Polish]. Klin Oczna 2005;107:668–71.
6. Miyake Y, Horiguchi M, Tomita N, et al. Occult macular dystrophy. Am J Ophthalmol 1996;122:644–53.
7. Ergun E, Hermann B, Wirtitsch M, et al. Assessment of central visual function in Stargardt's disease/fundus flavimaculatus with ultrahigh-resolution optical coherence tomography. Invest Ophthalmol Vis Sci 2005;46:310–6.
8. Wirtitsch E, Ergun B, Hermann A, et al. Ultrahigh resolution optical coherence tomography in macular dystrophy. Am J Ophthalmol 2005;140:976–83.
9. Drexler W, Sattmann H, Hermann B, et al. Enhanced visualization of macular pathology with the use of ultrahigh-resolution optical coherence tomography. Arch Ophthalmol 2003;121:695–706.
10. Ojima Y, Hangai M, Sasahara M, et al. Three-dimensional imaging of the foveal photoreceptor layer in central serous chorioretinopathy using high-speed optical coherence tomography. Ophthalmology 2007;114:2197–207.
11. Schocket LS, Witkin AJ, Fujimoro JG, et al. Ultrahigh-resolution optical coherence tomography in patients with decreased visual acuity after retinal detachment repair. Ophthalmology 2006;113:666–72.
12. Alam S, Zawadski RJ, Choi S, et al. Clinical application of rapid serial Fourier-domain optical coherence tomography for macular imaging. Ophthalmology 2006;113:1425–31.
13. Piccolino FC, de la Longrais RR, Ravera G, et al. The foveal photoreceptor layer and visual acuity loss in central serous chorioretinopathy. Am J Ophthalmol 2005;139:87–99.
14. Iida T, Hagimura N, Sato T, Kishi S. Evaluation of central serous chorioretinopathy with optical coherence tomography. Am J Ophthalmol 2000;129:16–20.
15. Pircher M, Baumann B, Gotzinger E, Hitzenberger CK. Retinal cone mosaic imaged with transverse scanning optical coherence tomography. Optics Lett 2006;15:1821–3.
16. Liang J, Williams DR, Miller DT. Supernormal vision and high-resolution retinal imaging through adaptive optics. J Opt Soc Am A Opt Image Sci Vis 1997;14:2884–92.
17. Roorda A, Williams DR. The arrangement of the three cone classes in the living human eye. Nature 1999;397:520–2.
18. Roorda A, Williams DR. Optical fiber properties of individual human cones. J Vis 2002;2:404–12.
19. Roorda A, Romero-Borja F, Donnelly W III, et al. Adaptive optics scanning laser ophthalmoscopy. Opt Express [serial online] 2002;10:405–12. Available at: http://www.opticsexpress.org/abstract.cfm?id=68843. Accessed March 11, 2008.
20. Pallikaris A, Williams DR, Hofer H. The reflectance of single cones in the living human eye. Invest Ophthalmol Vis Sci 2003;44:4580–92.
21. Wolfing JI, Chung M, Carroll J, et al. High-resolution retinal imaging of cone-rod dystrophy. Ophthalmology 2006;113: 1014–9.
22. Choi SS, Double N, Hardy JL, et al. In vivo imaging of the photoreceptor mosaic in retinal dystrophies and correlations with visual function. Invest Ophthalmol Vis Sci 2006;47: 2080–92.
23. Duncan JL, Zhang Y, Gandhi J, et al. High-resolution imaging with adaptive optics in patients with inherited retinal degeneration. Invest Ophthalmol Vis Sci 2007;48:3283–91.
24. Kitaguchi Y, Bessho K, Yamaguchi T, et al. In vivo measurements of cone photoreceptor spacing in myopic eyes from images obtained by an adaptive optics fundus camera. Jpn J Ophthalmol 2007;51:456–61.
25. Zawadzki RJ, Choi SS, Jones SM, et al. Adaptive optics-optical coherence tomography: optimizing visualization of microscopic retinal structures in three dimensions. J Opt Soc Am A Opt Image Sci Vis 2007;24:1373–83.
26. Douglas RS, Duncan J, Brucker A, et al. Foveal spot: a report of thirteen patients. Retina 2003;23:348–53.
27. Zambarakji HJ, Schlottmann P, Tanner V, et al. Macular microholes: pathogenesis and natural history. Br J Ophthalmol 2005;89:189–93.

Footnotes and Financial Disclosures

Originally received: November 25, 2007.
Final revision: March 16, 2008.
Accepted: March 25, 2008.
Available online: May 16, 2008. Manuscript no. 2007-1518.

[1] Department of Applied Visual Science, Osaka University Graduate School of Medicine, Osaka, Japan.

[2] Department of Ophthalmology, Osaka University Graduate School of Medicine, Osaka, Japan.

[3] Topcon Research Institute, Tokyo, Japan.

Financial Disclosure(s):
The funding organization had no role in the design or conduct of this research.

Supported by the Ministry of Health, Labor and Welfare, Tokyo, Japan (Health Sciences Research grant no.: H19-sensory-001).

Tatsuo Yamaguchi, Naoki Nakazawa, and Toshifumi Mihashi are employees of Topcon.

Correspondence:
Takashi Fujikado, MD, Department of Applied Visual Science, Osaka University Graduate School of Medicine, 2-2 Yamadaoka, Suita, Osaka 565-0871, Japan. E-mail: fujikado@ophthal.med.osaka-u.ac.jp.

Jpn J Ophthalmol 2008;52:380–385
DOI 10.1007/s10384-008-0575-1

CLINICAL INVESTIGATION

Photoreceptor Images of Normal Eyes and of Eyes with Macular Dystrophy Obtained In Vivo with an Adaptive Optics Fundus Camera

Kenichiro Bessho[1], Takashi Fujikado[1], Toshifumi Mihashi[2], Tatsuya Yamaguchi[2], Naoki Nakazawa[2], and Yasuo Tano[3]

[1]Applied Visual Sciences, Osaka University Graduate School of Medicine, Osaka, Japan; [2]Topcon Corporation Inc., Tokyo, Japan; [3]Department of Ophthalmology, Osaka University, Graduate School of Medicine, Osaka, Japan

Abstract

Purpose: To report on images of the human photoreceptor mosaic acquired in vivo with a newly developed, compact adaptive optics (AO) fundus camera.

Methods: The photoreceptors of two normal subjects and a patient with macular dystrophy were examined by using an AO fundus camera equipped with a liquid crystal phase modulator. In the eye with macular dystrophy, the fixation point in the AO images was identified using scanning laser ophthalmoscope (SLO) microperimetric image superimposed on a color fundus photograph.

Results: Photoreceptor cells were detected as bright dots approximately 4 μm in diameter in normal subjects. In the eye with macular dystrophy, the fixation point was located within the bull's eye lesion and uniform small whitish spots with irregular patchiness were observed in the AO images of this area. The distance between the small spots was 3–4 μm. In other parts of the bull's eye retinal lesion, the whitish spots were larger and of different sizes.

Conclusions: The photoreceptor mosaic could be identified in photographs of eyes of normal subjects and an eye with macular dystrophy in vivo by an AO fundus camera. In the eye with macular dystrophy, a relatively uniform photoreceptor mosaic was observed around the fixation point, whereas presumed debris of photoreceptor degradation was observed in the other bull's eye retinal lesion. **Jpn J Ophthalmol** 2008;52:380–385 © Japanese Ophthalmological Society 2008

Key Words: adaptive optics, cone mosaic, macular dystrophy, retinal imaging

Introduction

Adaptive optics (AO) technology, originally developed by astronomers to use with ground telescopes to compensate for atmospheric turbulence, has now been applied to fundus imaging. AO increases the resolution limits of retinal images by compensating for ocular wavefront aberrations.[1,2] Using an AO device, several studies have reported in vivo imaging of normal retinas[2–6] and the two-dimensional configuration of cone mosaic images. Recently, photoreceptor images from eyes with macular dystrophy have been obtained,[7,8] and a decrease of cone density was observed, which was correlated with a decrease in the amplitude of multifocal electroretinograms (ERGs). However, none of these reports referred to the fixation area in relation to the cone mosaic images.

The AO system consists of a wavefront sensor and a wavefront corrector, which form a closed loop of real-time wavefront compensation. The optical image with a reduced wavefront error is transferred to an imaging device such as a confocal scanning laser ophthalmoscope (SLO),[3] an optical coherence tomograph,[4] or a conventional fundus

Received: November 5, 2007 / Accepted: June 3, 2008
Correspondence and reprint requests to: Takashi Fujikado, Department of Applied Visual Sciences, Osaka University Graduate School of Medicine, 2-2 Yamadaoka, Suita, Osaka 565-0871, Japan
e-mail: fujikado@ophthal.med.osaka-u.ac.jp

camera.[1,2,5] The combination of a Hartmann-Shack wavefront sensor and a mechanical deformable mirror wavefront corrector seems to be the most widely used current AO system.

We developed a compact AO fundus camera using a Hartmann-Shack sensor and a liquid crystal wavefront modulator. We reported previously that our system could resolve individual photoreceptors in healthy eyes, and we have now used this system to measure interphotoreceptor spacing in both normal eyes and myopic eyes.[9]

Here we report another way in which our AO system can be applied. Our aim was to compare the AO images of a normal retina with those of an eye with macular dystrophy. More specifically, we examined whether the configuration of the cone mosaic in the fixation area differed from that in other areas within a bull's eye lesion.

Methods

Adaptive Optics System

A schematic diagram of the AO system is shown in Fig. 1. The main components of the system are a nematic liquid crystal phase modulator (LCPM; X8267-12, Hamamatsu Photonics, Hamamatsu, Japan), a Hartmann-Shack wavefront sensor (HSWS; 28 × 28 lenslets, especially made by Topcon, Tokyo, Japan), and a scientific charge-coupled device (CCD) digital camera (C9100-02, Hamamatsu Photonics). The light source for the wavefront sensing path was a 690-nm super luminescence diode (FiberMax, Blue Sky Research, Milpitas, CA, USA), and that for the retinal illumination path was a 635-nm laser diode (LLS-635–50, Moritex, Tokyo, Japan).

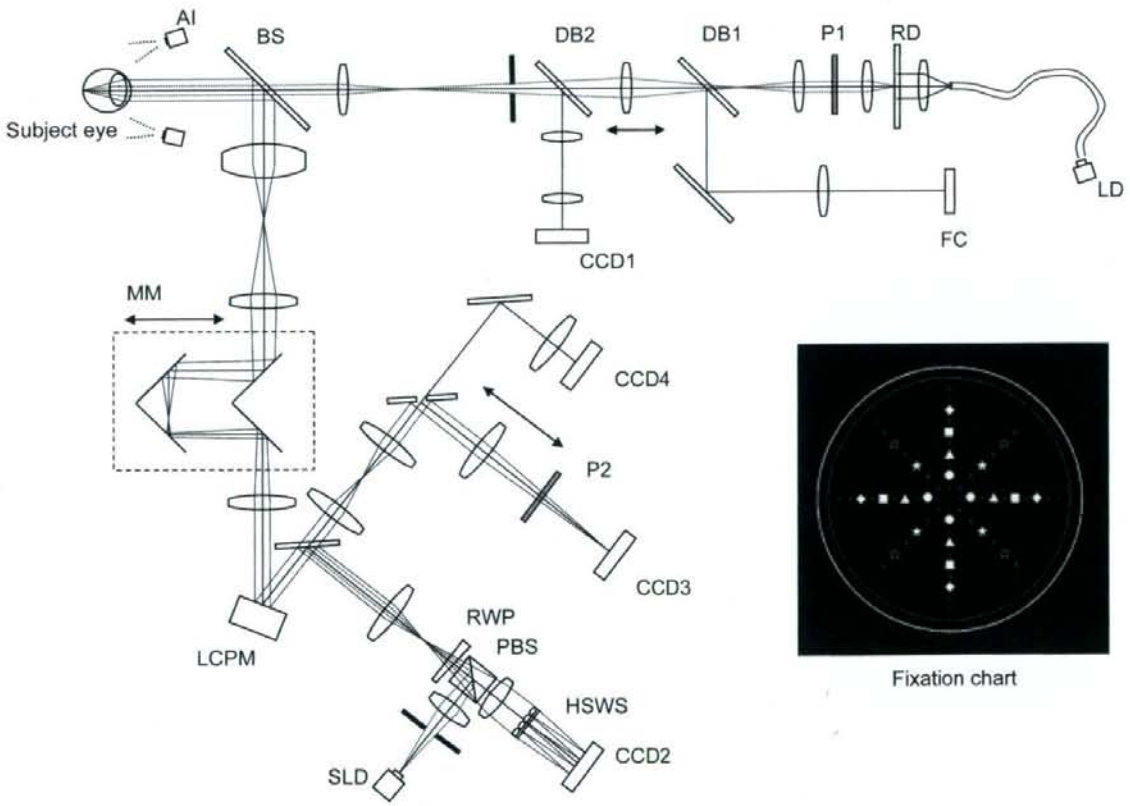

Figure 1. Schematic diagram of an adaptive optics fundus camera using a liquid crystal light modulator. AI, light source (LED 940 nm) for anterior segment illumination; *LD*, laser diode illuminator (635 nm); *SLD*, super luminescence diode illuminator (690 nm); *CCD*, charge-coupled device; *BS*, beam splitter; *DB1/DB2*, dichroic beam splitter; *FC*, fixation chart; *RD*, rotating diffuser; *P1*, *P2*, linear polarizers; *MM*, moving mirror; *RWP*, rotary wedged prism; *HSWS*, Hartmann-Shack wavefront sensor; *LCPM*, liquid crystal phase modulator (Hamamatsu PAL-SLM).

To avoid generation of speckles due to the coherence of the light sources, a rotary wedged prism was placed in the optical path of the HSWS, and a light-shaping diffuser sheet (LSD, Physical Optics, Torrance, CA, USA), which rotated at 20000 rpm in the retinal illumination path.

The HSWS measured the ocular wavefront up to the eighth Zernike order, and the LCPM compensated for the measured wavefronts. These two components formed a closed loop of continuous wavefront compensations, and operated at approximately 3 Hz, limited by the working speed of the LCPM. The system was also equipped with coaxial, 8° wide view optics to identify the location and orientation of the highly magnified retinal images observed. The area occupied by the AO system was 0.8 m × 0.8 m with a height of 25 cm, which might be compact enough to place in a clinical examination room. The entire AO system can be maneuvered by a single operator. Each series of AO images from the selected retinal locus can be captured in about 2 min, including targeting of the area, focusing, and wavefront compensation.

Subjects

A 40-year-old Japanese man presented with a progressive decrease of visual acuity over 20 years; his best-corrected visual acuity was 20/60 OU. Ophthalmoscopic examination revealed an annular zone of retinal pigment epithelial atrophy in the macula (bull's eye maculopathy) in both eyes (Fig. 2). His younger brother had a similar macular lesion. Bilateral ring scotomas were detected in both eyes of the patient by Goldmann perimetry. A moderate window defect without leakage was observed in the macular area by fluorescein angiography. The 30-Hz flicker ERGs and flash ERGs were of normal amplitude.

Two healthy volunteers (a 38-year-old man and a 31-year-old woman) were also examined.

Image Capturing

The research protocols were approved by the institutional review board of Osaka University Medical School and conformed to the tenets of the Declaration of Helsinki. After the nature and possible consequences of the study were explained, written informed consent was obtained from the two subjects and the patient.

After the pupils were dilated by topical 0.5% tropicamide and 0.5% phenylephrine, the examinee was seated in front of the AO system with a regular chin rest and asked to fixate the target. A retinal photograph was taken by the CCD as a 20-frame movie sequence with 10-bit grayscale images (1000 × 1000 pixels) and the total root mean square (RMS) error was reduced below the preset trigger value (usually 0.10 μm for a 5-mm pupil). The magnification of the image was calculated from the axial length of the eye.[10]

In the macular dystrophy patient, the retinal locus of fixation was verified by microperimetry using a confocal SLO (Rodenstock SLO ver 1.0, Rodenstock, Munich, Germany),[11] conventional color fundus photographs (Topcon TRC50LX, Topcon), and optical coherence tomography (OCT3000, Carl Zeiss Meditec, Dublin, CA, USA). The mosaic AO image was manually processed with Adobe Photoshop CS1 (Adobe, San Jose, CA, USA) image-processing software. With the same software, the color fundus image and the SLO image were superimposed on the mosaic AO image and the retinal locus of fixation in the AO image was determined.

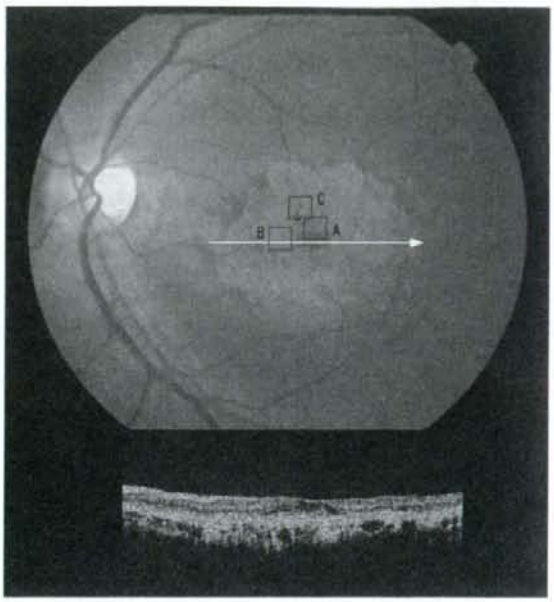

Figure 2. Fundus and optical coherence tomography (OCT) images of the left eye of a patient with macular dystrophy. The *blue cross* represents the fixation point, verified by the scanning laser ophthalmoscope microperimetry. The *white arrow* shows the position of the OCT transect. The *square boxes* represent the areas examined by adaptive optics (AO) and are labeled with *letters* corresponding to the parts of Fig. 4.

Calculation of the Cone Density

Cone density was calculated in three steps.

1. Image processing of each grabbed image before image summation using the deconvolution function, "deconvlucy," of MATLAB (Mathworks, Natick, MA, USA) was performed to get a clear separation of the cones.
2. Image summation to improve the signal-to-noise ratio was performed using our original program. The number of superimposed images ranged from 8 to 64 frames, depending on the imaging conditions.
3. The cones were marked. Retinal loci about 2° temporal of the center of the fovea were examined. Three 100 μm

× 80 μm rectangular areas were selected, excluding those in which retinal vessels had a cone mosaic that required degrading. Bright spots 2–5 μm in diameter were considered to be cones. A single examiner (KB) manually marked the cones in the target area. The examiner used the accented edges function of Photoshop CS1 whenever this function made the task easier. However, even when this function was used, the final identification of the cone was always done by observing the original averaged image.

Results

In both the volunteers and the patient, the ocular aberration was reduced to below 0.1 μm RMS (Table 1). In the two normal subjects, the photoreceptors were imaged as slightly oval-shaped bright dots with a tiled packing arrangement (Fig. 3; the AO image of normal subject 2 is not shown). The diameter of the bright dot was approximately 4 μm, and the density was 40 950/mm^2 and 54 530/mm^2 at 2° from the fovea centralis. These values are comparable to those obtained by another histological study of the human cone mosaic (40 000–50 000/mm^2).[12]

In the eye with macular dystrophy, the visual field obtained by the SLO microperimetry showed a ring scotoma. The fixation point was located within the bull's eye lesion and was approximately 200 μm superonasal from a central dark area (Fig. 2). The OCT images showed cystic changes in the fovea and degenerative changes of the retinal pigment epithelium in the macular area, but the precise degree of photoreceptor degeneration could not be determined.

In the AO retinal image, the observed morphology of the photoreceptor layer varied considerably, suggesting degeneration of the photoreceptors (Fig. 4). No structure was observed in the central dark area, and the shape of the white dots in the surrounding bright-colored area varied widely (Fig. 4A). Relatively uniform white dots were observed at several loci in the same area.

In the area where the white dots were uniformly distributed, the distance between spots was 3–4 μm, comparable

Table 1. Profiles of subjects

	Normal 1	Normal 2	Patient
Sex	Male	Female	Male
Age (years)	38	31	40
Imaged eye	OS	OS	OS
Retinal status	No disease	No disease	Macular dystrophy
BCVA	20/15	20/20	20/60
Subjective refraction	Sph-1.0 D Cyl-0.3 D	Sph-0.9 D Cyl-0.2 D	Sph-1.8 D Cyl-0.8 D
RMS[a] without AO (μm)	0.317	0.213	0.306
RMS with AO (μm)	0.083	0.078	0.094
Average cone density[b] (cones/mm^2)	40950	54530	ND

BCVA, best-corrected visual acuity; RMS, root mean square; AO, adaptive optics; ND, not done.

[a]Root mean square value of aberration coefficients of the second to eighth Zernike order for a 5-mm pupil diameter. The 2° temporal from the fovea was measured.

[b]Calculated from the cone spacing in the area 2° temporal from the fovea.

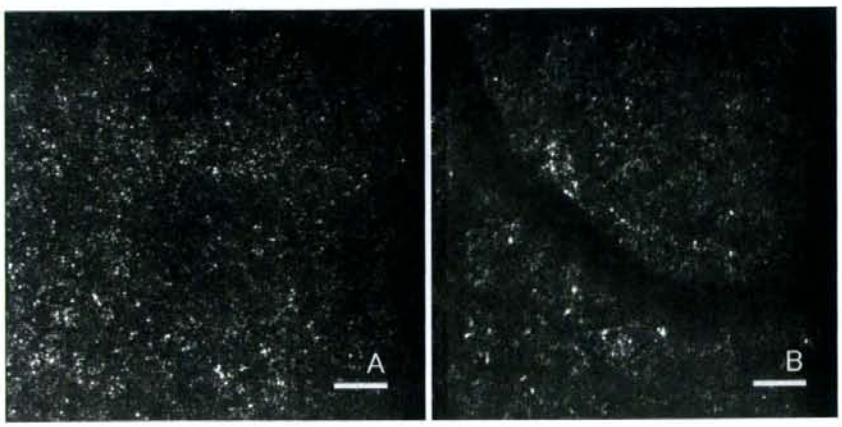

Figure 3A, B. AO image of a normal subject. Deconvolution was performed by using residual wavefront error data and subsequently five frames were averaged. **A** Center of the macula. The image covers the foveal avascular zone. The foveal center appears relatively darker than the surrounding area. **B** Three degrees temporal to the foveal center. Bar = 50 μm.

Jpn J Ophthalmol
Vol 52: 380–385, 2008

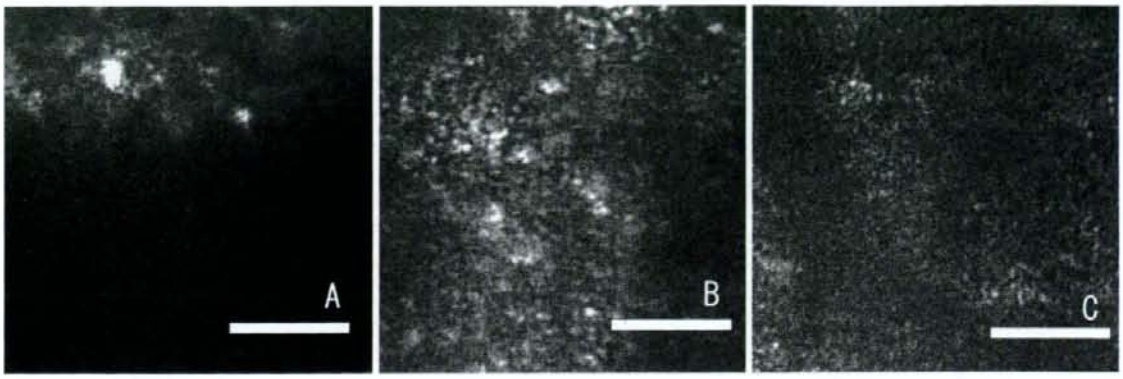

Figure 4A–C. Individual AO images of the sampled areas. The orientation of each image was determined by creating a composite AO image and registering it on the color fundus picture in Fig. 2. The letters correspond to the labeled sampling areas in Fig. 2. The total residual root mean square wavefront error was 0.089, 0.090, 0.162 μm for **A–C**, respectively, for a 5-mm pupil. **A** Upper edge of the central dark area. Very large irregular spots are seen above the dark area. **B** Example of an image with large, scattered, irregular spots. **C** Area near the locus of fixation. The dark vertical streak represents a capillary vessel. A patchy dark area is also seen on the right side of the image. Bar = 50 μm.

to that in the normal eyes and consistent with the interphotoreceptor distance obtained from histological data.[12]

In the nonuniform area, the bright spots were larger, ranging from 2 to 20 μm, and less uniform than those in the normal retinas, in which photoreceptors appeared as uniform small spots of 2–5 μm (Fig. 4B).[12] In the fixation area, the spots were more uniform in size and the overall appearance was more similar to normal retinas (Fig. 4C).

Discussion

The AO system used in this study is equipped with an LCPM as a wavefront corrector instead of the deformable mirror used in other AO systems. In our previous study we showed that this compact AO system can still effectively resolve cone photoreceptors. On the other hand, the LCPM has several limitations. The current system operates at approximately 3 Hz; thus, eye movement can affect the image quality. In this study, all subjects, including the macular dystrophy patient, had good fixation as judged from the AO images in the movie sequence, so the eye movement may not have been significant. We selected a 690-nm laser diode as the illuminator in order to reduce glare during the examinations. Because the coherence of this illuminator causes speckles, we used a rotating diffuser. Another problem may be that the LCPM can modulate only polarized light. This means that with this system we could obtain only partial optical information from the retina, which might be a problem when precise optical properties of retinal microstructures are studied, but we believe that the system is still applicable to the study of two-dimensional photoreceptor arrangements or photoreceptor morphology.

In the normal subjects, it was possible to obtain clear images of the photoreceptors with good wavefront compensation (Fig. 2). In this study, the calculated size of each spot was 2–5 μm, consistent with that obtained by other studies using a high-resolution system[13] or OCT[14] and by histological studies.[12]

In the eye with macular dystrophy, several patterns of AO image were seen in the bull's eye lesion. A central dark-colored area was uniform without structure. This may indicate either that a disorder of the inner retinal layers blocked the image or that the photoreceptors in this area are absent.

In the surrounding rough bright-colored area, scattered white spots of different shapes and sizes were seen. As this area showed reduced retinal sensitivity in SLO microperimetry, these spots may represent either morphologically changed photoreceptors or photoreceptor degeneration debris (Fig. 4).[8]

The fixation point on the retina was also located in the surrounding rough bright-colored area. The AO image showed a rather uniform distribution of white spots whose separation was consistent with the cone mosaic. It is possible that the photoreceptors were less affected in the fixation area.

The image obtained using the AO system is not fully understood. The spots in the AO images might be inner segment–outer segment (IS/OS) photoreceptor junctions because in the normal retina each spot seems to be in a one-to-one correspondence with a single photoreceptor, and because recent studies using high-resolution OCT suggest that the IS/OS junction seems to show its highest reflectivity inside the photoreceptor layer.[15] At the same time, it has been observed that this IS/OS reflection tends to disappear and reappear during the course of retinal diseases such as serous macular detachment[16] or macular hole, indicating that the IS/OS reflection probably indicates a functional aspect of the photoreceptors and that loss of the IS/OS reflection does not necessarily mean the absence of

the photoreceptor itself. Considering this, we note that the absence of regular spots does not necessarily mean the absence of photoreceptors, but it may indicate a functional change in the photoreceptors. In the same way, irregular spots, too, may be signs of a functional change in the photoreceptors. It may be possible to learn more about this issue by a study combining AO fundus camera and high-resolution OCT images.

Although our AO system has several limitations, we have shown that a two-dimensional image of photoreceptor cells can be obtained that is useful for examining macular dystrophy. In the future, animal studies are needed to investigate the origin of the large spots, and studies to improve the resolution of the AO system for quantitative evaluation of residual photoreceptors in diseased retinas are also needed.

Acknowledgments. Kenichiro Bessho and Takashi Fujikado had full access to all data in the study and take responsibility for the integrity of the data and the accuracy of the data analysis. This study was supported by a Health Sciences Research Grant (H19-sensory-001) from the Ministry of Health, Labour and Welfare, Japan

References

1. Liang J, Williams DR, Miller DT. Supernormal vision and high-resolution retinal imaging through adaptive optics. J Opt Soc Am A 1997;14:2884–2892.
2. Roorda A, Williams DR. The arrangement of the three cone classes in the living human eye. Nature 1999;397:520–522.
3. Roorda A, Romero-Borja F, Donnelly WJ III, et al. Adaptive optics scanning laser ophthalmoscopy. Opt Express 2002;10: 405–412.
4. Hermann B, Fernandez EJ, Unterhuber A, et al. Adaptive-optics ultrahigh-resolution optical coherence tomography. Opt Lett 2004;29:2142–2144.
5. Doble N, Yoon G, Chen L, et al. Use of a microelectromechanical mirror for adaptive optics in the human eye. Opt Lett 2002;27: 1537–1539.
6. Roorda A, Metha AB, Lennie P, Williams DR. Packing arrangement of the three cone classes in primate retina. Vision Res 2001;41:1291–1306.
7. Wolfing JI, Chung M, Carroll J, et al. High-resolution retinal imaging of cone-rod dystrophy. Ophthalmology 2006;113: 1014–1019.
8. Choi SS, Doble N, Hardy JL, et al. In vivo imaging of the photoreceptor mosaic in retinal dystrophies and correlations with visual function. Invest Ophthalmol Vis Sci 2006;47:2080–2092.
9. Kitaguchi Y, Bessho K, Yamaguchi T, et al. In vivo measurements of cone photoreceptor spacing in myopic eyes from images obtained by an adaptive optics fundus camera. Jpn J Ophthalmol 2007;51: 456–461.
10. Bennett AG, Rudnicka AR, Edgar DF. Improvements on Littmann's method of determining the size of retinal features by fundus photography. Graefes Arch Clin Exp Ophthalmol 1994;232: 361–367.
11. Oyagi T, Fujikado T, Hosohata J, et al. Foveal sensitivity and fixation stability before and after macular translocation with 360-degree retinotomy. Retina 2004;24:548–555.
12. Curcio CA, Sloan KR, Kalina RE, Hendrickson AE. Human photoreceptor topography. J Comp Neurol 1990;292:497–523.
13. Miller DT, Williams DR, Morris GM, Liang J. Images of cone photoreceptors in the living human eye. Vision Res 1996;36: 1067–1079.
14. Pircher M, Baumann B, Gotzinger E, Hitzenberger CK. Retinal cone mosaic imaged with transverse scanning optical coherence tomography. Opt Lett 2006;31:1821–1823.
15. Zawadzki RJ, Choi SS, Jones SM, et al. Adaptive optics-optical coherence tomography: optimizing visualization of microscopic retinal structures in three dimensions. J Opt Soc Am A Opt Image Sci Vis 2007;24:1373–1383.
16. Ojima Y, Hangai M, Sasahara M, et al. Three-dimensional imaging of the foveal photoreceptor layer in central serous chorioretinopathy using high-speed optical coherence tomography. Ophthalmology 2007;114:2197–2207.

Clinical & Experimental Ophthalmology

Clinical and Experimental Ophthalmology 2008; **36**: 861–864
doi: 10.1111/j.1442-9071.2008.01903.x

Clinicopathological Report

Vitreous surgery for macular hole in patients with Vogt-Koyanagi-Harada disease

Izumi Kobayashi MD,[1] Makoto Inoue MD,[1] Annabelle A Okada MD,[1] Hiroshi Keino MD,[1] Toshiko Wakabayashi MD[1,2] and Akito Hirakata MD[1]
[1]Kyorin Eye Center, Kyorin University School of Medicine, and [2]Kanto Medical Center NTT EC, Tokyo, Japan

Abstract

We describe two patients with Vogt-Koyanagi-Harada (VKH) disease, both in the convalescent stage, who presented with unilateral macular holes together with clinically significant epi-retinal membranes. Vitreo-retinal surgery was performed on the affected eyes and the surgical technique involved a standard three-port vitrectomy, peeling of the epi-retinal and internal limiting membrane (ILM). In both cases the retinae were tamponaded with air resulting in anatomical closure of the macular holes. The histology of the excised membrane was available in one case and this revealed multiple layers of presumed retinal pigment epithelial cells with cytoplasmic processes and intercellular junctions forming a basal lamina attached to the smooth surface of the ILM. Our findings demonstrate that macular holes can develop in patients with VKH but that the hole can be successfully closed with vitreo-retinal surgery. The convalescent stage tends to occur several weeks after the acute stage when the uveitic process has subsided and is characterized by choroidal depigmentation, producing a sunset glow appearance to the ocular fundus. Patients may also demonstrate varying degrees of cutaneous hypopigmentation, poliosis and/or alopecia. Macular holes have also been reported previously in patients during the convalescent stage of VKH and this communication describes the outcome of two patients who underwent vitreo-retinal surgery for this problem.

Key words: electron microscopy, epiretinal membrane, macular hole, vitreous surgery, Vogt-Koyanagi-Harada disease.

Introduction

Vogt-Koyanagi-Harada (VKH) disease is an inflammatory disorder affecting the eyes, auditory system, meninges and skin.[1–2] Patients at the acute stage may have auditory and neurological manifestations including severe headaches and meningismus, followed by visual deterioration associated with bilateral exudative retinal detachment and optic disc hyperemia.[3] Patients at the convalescent stage have ocular signs and symptoms of bilateral anterior uveitis with sunset glow fundi, in the absence of exudative retinal detachment. They may also have varying degrees of cutaneous hypopigmentation, poliosis and/or alopecia.

A VKH patient who had developed a macular hole after posterior vitreous detachment (PVD) during the convalescent stage was described to achieve limited visual improvement after two surgical procedures to close the macular hole.[4] We describe two patients with VKH disease who developed a macular hole during the convalescent stage, and vitrectomy with removal of the internal limiting membrane (ILM) led to a successful closure of the macular holes.

Case reports

Case 1

A 62-year-old Japanese woman presented with decreased vision in the left eye. She had been diagnosed with VKH disease 2 years earlier and was on a maintenance dose of 100 mg/day of oral cyclosporine. Prior to developing VKH, this patient had been treated with laser photocoagulation because of bilateral branch vein occlusions. The patient at presentation was pseudophakic in each eye, her presenting acuities were 6/9 right eye (OD) and 6/30 left eye (OS). Both eyes were white and quiet and ophthalmoscopy revealed sunset glow fundi and peripheral nummular chorioretinal depigmented scars bilaterally (Fig. 1a,b). A thick epiretinal membrane and a stage 3 macular hole without a PVD were observed in the left eye (Fig. 1b,d). The patient was diagnosed with a macular hole associated with VKH disease in the convalescent stage.

■ *Correspondence:* Dr Makoto Inoue, Kyorin Eye Center, Kyorin University School of Medicine, 6-20-2 Shinkawa, Mitaka, Tokyo 181-8611, Japan. Email: inoue@eye-center.org

Received 24 July 2008, accepted 5 November 2008.

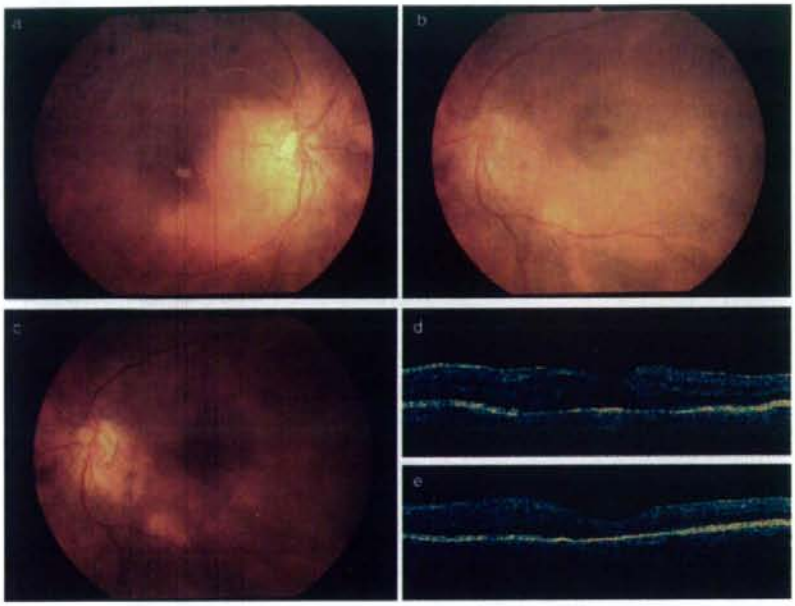

Figure 1. Fundus photographs and optical coherence tomography (OCT) images of Case 1. (a) Fundus photograph of the right eye showing sunset glow fundus with scars of laser photocoagulation related to a previous branch retinal vein occlusion. (b) Fundus photograph of the left eye showing sunset glow fundus with epiretinal membrane and a stage 3 macular hole. (c) Postoperative fundus photograph of the left eye showing closure of the macular hole and absence of the epiretinal membrane. (d) Preoperative OCT horizontal image showing a macular hole of a flattened inner retinal surface presumably due to contraction of an epiretinal membrane. (e) Postoperative OCT horizontal image showing complete closure of the macular hole.

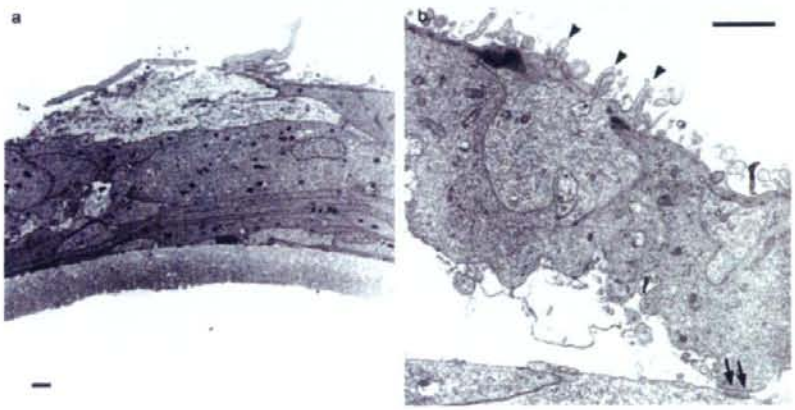

Figure 2. Electron microscopic analysis of the excised membrane from Case 1. (a) Low magnification electron photomicrograph of the excised epiretinal membrane showing multiple layers of cells on the surface of the ILM (bar, 1 μm). (b) Higher magnification electron photomicrograph of the excised epiretinal membrane shows cytoplasmic processes (arrowheads) and intercellular junctions forming a basal lamina (arrows), suggesting that these cells are retinal pigment epithelial cells (bar, 1 μm).

Vitrectomy was performed with 25-gauge instruments. A PVD was created, and an epiretinal membrane that was firmly attached to the macula was removed. Then the ILM was peeled off of the retina. Fluid/air exchange was performed for air tamponade, and the patient was instructed to maintain a face-down position for 3 days.

Postoperatively, the macular hole was closed as confirmed by optical coherence tomography (OCT; Stratus OCT, Carl Zeiss Meditec, Dublin, CA, USA, Fig. 1c,e). Visual acuity improved to 6/9 at one month, after which the patient returned to her local ophthalmologist for continued follow up of the VKH disease.

Electron microscopic examination of the excised membrane revealed multiple layers of cells on the surface of the ILM (Fig. 2a). High magnification of the cells showed cytoplasmic processes and intercellular junctions forming a basal lamina, suggestive of retinal pigment epithelial (RPE) cells (Fig. 2b).

Case 2

A 60-year-old Japanese man presented with decreased vision in the left eye. He had been diagnosed with VKH disease approximately 20 years earlier with baseline visual acuities of

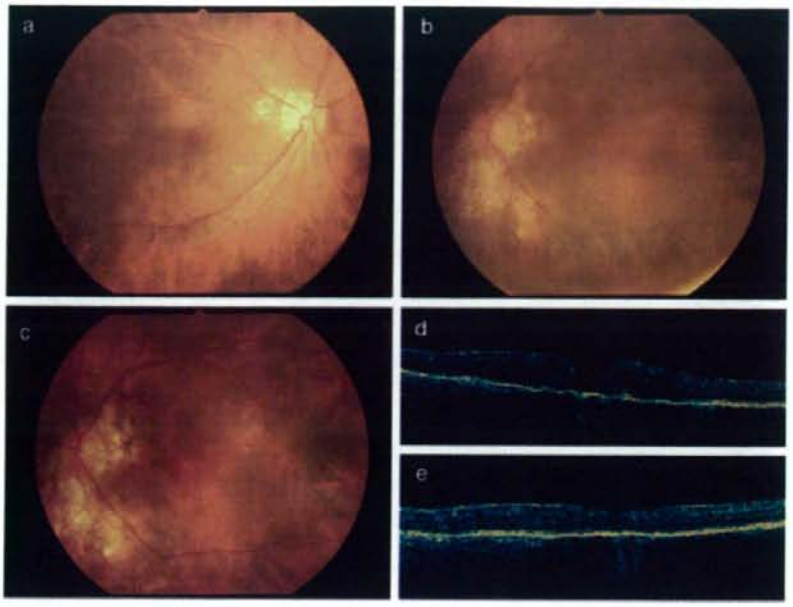

Figure 3. Fundus photographs and optical coherence tomography (OCT) images of Case 2. (a) Fundus photograph of the right eye showing sunset glow fundus. (b) Fundus photograph of the left eye showing sunset glow fundus with epiretinal membrane and a stage 3 macular hole. (c) Postoperative fundus photograph of the left eye showing closure of the macular hole and absence of the epiretinal membrane. (d) Preoperative OCT horizontal images showing a macular hole and a flattened inner retinal surface presumably due to contraction of the epiretinal membrane. (e) Postoperative OCT horizontal images showing complete closure of the macular hole.

6/6 OD and 6/9 OS. He was still being followed on topical dexamethasone drops by a local ophthalmologist. His presenting acuities were 6/6 OD and 6/19.8 OS. Both eyes were white and quiet with bilateral moderate cataract and ophthalmoscopy revealed sunset glow fundi and peripheral nummular chorioretinal depigmented scars bilaterally (Fig. 3a,b). An epiretinal membrane and a stage 4 macular hole with a PVD were observed in the left eye (Fig. 3b,d). The patient was diagnosed with VKH disease at the convalescent stage accompanied by a macular hole.

Vitrectomy was performed as done in Case 1. An epiretinal membrane that was firmly attached to the macula was removed together with ILM. Postoperatively, the macular hole was closed as confirmed by OCT, and the visual acuity improved to 6/15 3 months after surgery (Fig. 3c,e).

Discussion

Macular hole is believed to develop due to traction on the macula by adherent vitreous, particularly in eyes with cystoid macular edema caused by chronic intraocular inflammation.[4] Nevertheless, a macular hole is a relatively rare complication of uveitis.[5] Electron microscopic analysis of excised membrane suggested that RPE cells had migrated and proliferated on the ILM in the eye of one of our patients. These RPE cells may contribute to the formation of macular hole by adhering to the vitreous cortex and contracting. This differs from the ultrastructural features of the vitreoretinal interface of eyes with a macular hole without intraocular inflammation. In these cases, there is a glial cell-dominant proliferation onto the ILM.[6]

The question then arises on whether there is a causal relationship between the macular hole and VKH disease in our two patients. In both of our cases, an epiretinal membrane was present, and traction by this membrane was most likely the cause of the macular hole. Presence of RPE-like cells on the surface of the ILM in the excised membrane of the cases is in keeping with earlier findings of RPE cells on the ILM obtained from eyes with macular pucker.[7] Although both of the eyes were at the convalescent stage, the earlier uveitis may have led to the migration of RPE cells to the ILM, and the changes observed were manifested at the convalescent stage.

Quantitative analyses showed that the changes in the sunset glow fundus progress over the first 3–6 months after the onset of disease, even in the absence of obvious intraocular inflammation.[8] As might be expected, eyes with chronic inflammation show a faster progression of the sunset glow appearance than eyes without chronic inflammation.[9] These findings suggest a persistent subclinical inflammation in some eyes at the convalescent stage, which may account for the migration and contraction of the RPE cells.

In summary, a macular hole may develop in VKH patients at the convalescent stage, and vitreous surgery is effective in closing the macular hole.

Acknowledgements

The authors received no financial support in reporting these clinical observations. The corresponding author (MI) had full access to all the data in the study and takes responsibility for the integrity of the data and the accuracy of the data analysis.

REFERENCES

1. Rao NA, Inomata H, Moorthy RS. Vogt-Koyanagi-Harada syndrome. In: Pepose J, Holland GN, Wilhelmus K, eds. *Ocular Infection and Immunity*. St Louis, MO: Mosby-Year Book, 1996; 734–53.
2. Moorthy RS, Inomata H, Rao NA. Vogt-Koyanagi-Harada syndrome. *Surv Ophthalmol* 1995; **39**: 262–92.
3. Read RW, Holland GN, Rao NA *et al.* Revised diagnostic criteria for Vogt-Koyanagi-Harada disease: report of an international committee on nomenclature. *Am J Ophthalmol* 2001; **131**: 647–52.
4. Kawamura R, Okuda E, Shinoda H *et al.* A case of macular hole developed in the convalescent stage of Vogt-Koyanagi-Harada disease. *Jpn Rev Clin Ophthalmol* 2003; **97**: 1081–4.
5. Angioi-Duprez K, Maalouf T, Gerin M, George JL. A full thickness macular hole as an uncommon complication of Behcet disease. *J Fr Ophtalmol* 2001; **24**: 154–9.
6. Schumann RG, Schaumberger MM, Rohleder M *et al.* Ultrastructure of the vitreomacular interface in full-thickness idiopathic macular holes: a consecutive analysis of 100 cases. *Am J Ophthalmol* 2006; **141**: 1112–9.
7. Lindsey PS, Michels RG, Luckenbach M, Green WR. Ultrastructure of epiretinal membrane causing retinal starfold. *Ophthalmology* 1983; **90**: 578–83.
8. Suzuki S. Quantitative evaluation of 'sunset-glow' fundus in Vogt-Koyanagi-Harada disease. *Jpn J Ophthalmol* 1999; **43**: 327–33.
9. Keino H, Goto H, Usui M. Sunset glow fundus in Vogt-Koyanagi-Harada disease with or without chronic ocular inflammation. *Graefes Arch Clin Exp Ophthalmol* 2002; **240**: 878–82.